# An improved prescribed performance control for the attitude tracking control of hypersonic vehicle with uncertain disturbances

Yaokun Zhang[1]

*Radarweg 29, Amsterdam*

*Elsevier Inc[1], Global Customer Service[b,*]*

*[a]1600 John F Kennedy Boulevard, Philadelphia*
*[b]360 Park Avenue South, New York*

**Abstract**

Nowadays the comprehensive control performance with the expected transient response and specified steady-state accuracy is increasingly emphasized in the flight control field, to which the prescribed performance control (PPC) is a very suitable solution. Aiming at the defects of conventional PPC in practical engineering, an improved PPC method and its application in the attitude tracking control of a generic hypersonic vehicle (GHV) are presented in this paper. The novel approach develops an adaptively alterable performance constraint scheme, which reduces dependence on the prior knowledge of control error and is more flexible for performance presetting. Moreover, a performance constraint resetting mechanism is exploited to solve the potential performance transgression problem and enhance the anti-disturbance ability of the control system. Besides, a simple dual-loop integral sliding mode controller combined with the novel PPC is designed based on the nonlinear dynamical model of GHV. Numerical simulations in both pitch maneuver control and three-channel attitude tracking control cases indicate the feasibility and superiority of the new design.

⋆Fully documented templates are available in the elsarticle package on CTAN.

*Corresponding author
*Email address:* support@elsevier.com (Global Customer Service)
*URL:* www.elsevier.com (Elsevier Inc)

[1]Since 1880.

*Keywords:* Generic hypersonic vehicle, Attitude tracking control, Prescribed performance control, Comprehensive control performance

## 1. Introduction

The attitude tracking control problem of modern high-speed aircraft is a hot research topic in the field of flight control. With the rapid development of related fields, the flying speed of aircraft is getting faster and faster, and the flying airspace is becoming larger and larger, resulting in the more complicated flight environment and stronger nonlinearity and uncertainty in the flight control system, in which condition, the conventional flight control schemes get a bit difficult to achieve satisfactory control performance. On the other hand, although the stability of the system is always the first for the flight control, more and more new flight missions, such as aerial refueling, precise strike, and fast maneuvering, etc., place higher requirements on the comprehensive performance of flight control, namely, the control system is expected to track flight attitude commands more quickly and accurately while maintaining stability and the expected transient re-sponse and specified steady-state accuracy are even re-quired sometimes[1, 2]. Therefore, it is of great significance to pay more attention to the comprehensive control per-formance of the flight control.

For the attitude tracking control of aircraft, from the perspective of linear control, practical engineering largely employes the schemes of the gain-scheduled control [3] or the multiple model control [4], which are safe and practical enough but often appear to be time-consuming, cumbersome, and unsatisfactory. And from the perspective of nonlinear control, there are more representative design methods including dynamic inversion control[5], backstepping control[6, 7], robust control[8, 9], sliding mode control[10–12] and adaptive control[6, 7, 10, 11], etc., in which studies, the emphasis of the control design are mainly on the stability and robustness of the control system, that is how to stabilize a system or how to adjust the convergence bounds of the control error. However, for the purpose of improving the comprehensive control performance of the control

system, some problems exist in the research of these control methods:

- On the one hand, to deal with the inevitable uncertain disturbances (including uncertainty of model parameters, unmodeled dynamics and external disturbances), the most direct method is to enhance the robustness of the control system, but conventional robust control methods will sacrifice the dynamic performance of the system, which is not expected. Therefore, many studies have adopted more proactive coping strategies, such as designing disturbance observers[5, 12, 13] or using neural system[6, 14, 15] or fuzzy system[11, 16, 17] to approximate uncertain terms and compensate for disturbances, which have achieved good results to a certain extent, but the addition of a variety of complex technologies makes the system cumbersome, difficult to debug and easy to malfunction in practical applications.

- On the other hand, the transient control performance of the control system, such as overshoot and error convergence rate, which are sometimes of equal importance with steady-state performance, are often less considered. Actually, there have been some remarkable researches on the rapidity of nonlinear control, such as the finite-time convergence[18, 19], and the fixed-time convergence[20], but in general, the existing dominant flight control methods are not specially developed for comprehensive performance: either these methods only meet some single performance requirements or the control performance cannot be accurately quantified.

In the last few decades, many scholars have continuously made exploratory research work regarding the comprehensive control performance of the nonlinear systems. As early as 1991, the concept of "good transient performance response" was given in Ref.[21]. Then, a "performance channel" described by the functional differential equation in Ref.[22] was used to restrict the dynamic response of the system to achieve the convergence of tracking error within a predefined performance channel. Furthermore, in Refs.[23, 24], the prescribed performance control (PPC) theory was first proposed, which incorporates the

desired performance indicators as constraints into the design of the controller, thereby transforming this problem to a control problem with performance constraints. Subsequently, a large number of scholars combined this theory with existing control methods to develop some new design schemes with performance guaranties, which had shown a good application prospect in the field of robotic engineering [25, 26], power system[27] and flight control [28–30]. Although there have been many remarkable studies on the PPC, it is still necessary to take some effort to improve this method, especially for its application in flight control.

- First of all, the emphases of the most existing studies in PPC fall on the control design based on prescribed performance theory to improve the system's transient performance [31, 32], but they rarely involve the performance prescribing scheme, which is inflexible for a real system in the conventional PPC design.

- Secondly, the initial error of the system is required as prior knowledge to determine the parameters of performance constraints in the conventional PPC design, however, the actual control error is always unpredictable in a real system due to the complex and changing environment, which makes it limited to conduct this method in the practical applications. To avoid this trouble, a novel performance function with infinite initial boundaries is developed for the velocity and altitude control of the hypersonic vehicle in Ref.[33] so that the initial error is needless and a unified formula can be used for both cases of the positive and negative errors.

- Thirdly, for some unexpected cases (such as strong external interference, system failure or dramatical change of the reference input, etc.), or due to the improper setting of the performance boundary, the control error of the actual system may overrun the preset error bounds, which is named as "performance transgression" in this paper. This potential threat will adversely affect the stability of the system but is scarcely considered in the conventional PPC. In Ref.[34], a concept of the switched prescribed performance with multiple performance functions is proposed to develop

an adjustable PPC method for the performance transgression problem in the high angle of attack maneuver control, which can appropriately adjust the performance constraints in real-time, however, this new method will break the preset performance constraints and is complicated to operate. In Ref.[35], by introducing the derivative of the reference input, a novel performance function is designed to solve the problem of initial error dependence and prevent overrun of control inputs when the reference input change drastically at the steady-state, in which, the only catch is that the paper mainly studies the input nonlinearity with unknown dead zone and the flexible dynamics of the hypersonic vehicle, but ignores the external interference in flight.

Aiming at the above problems, this paper makes some different improvements to the conventional PPC and applies the proposed new PPC method to the attitude tracking control of the hypersonic vehicle. The special contributions of this paper are summarized as follows:

(1) A novel performance constraint scheme with adaptively alterable constraint is proposed, which not only reduces dependence on the prior knowledge of control error but also can adaptively set the range of constraint boundary according to the actual error. In this way, the performance presetting can be more flexible, and higher control accuracy can be achieved while satisfying the prescribed performance. And compared with the existing improvement schemes [33–35], the performance function has a more simple and clear form in this proposed new method.

(2) A performance constraint resetting mechanism is proposed for the first time to solve the potential performance transgression problem and enhance the anti-disturbance ability of the control system, which makes this method more practical for the real applications.

(3) A dual-loop integral sliding mode controller combined with the proposed novel PPC is designed for the attitude tracking control of a generic hypersonic vehicle (GHV). This control scheme does not involve any complicated

observer or neural network structure, but it can still effectively deal with various uncertain disturbances during flight, which is simple and practical enough to be a new idea to solve the uncertainty in the flight control.

(4) Different from simulations in the general studies of flight control, Numerical simulation experiments in both pitch maneuver control and six-DOF three-channel attitude tracking control cases are carried out in this paper to fully validate the feasi-bility and superiority of the new scheme.

The structure and main contents of the rest of this paper are as follows. Section II introduces the nonlinear dynamical model of the GHV and the basic theory of PPC. Section III describes the improved prescribed performance scheme and the controller design using the sliding mode control method. In section IV, abundant numerical simulations are presented to show the effectiveness and practicability of the proposed method. Some conclusions are finally drawn in Section V.

## 2. Problem formulation and preliminaries

### *2.1. Dynamical model of GHV*

A generic hypersonic vehicle model, published by NASA, named "winged-cone", is selected as the research object [36]. To model and analyze the motion of the GHV, some frames are firstly defined as shown in Fig. 1, including the earth-fixed inertial reference frame (ERF), the vehicle body-fixed reference frame (BRF), the flight path reference frame (TRF). The angle of attack, sideslip angle and the roll angle of the velocity in TRF constitute attitude control vector $\Theta = [\alpha, \beta, \mu]^T$, the angular rates of the pitch, yaw, and roll in BRF constitute attitude angular rate control vector $\boldsymbol{\omega} = [q, r, p]^T$.

The unpowered reentry flight of the GHV is mainly focused in this paper, in which phase, the parameters of the mass, the center of mass, and the moment of inertia of GHV can be considered unchanged. Besides, since the GHV is plane symmetrically structured, the inertia tensor matrix can be simplified to $\mathbf{J} = diag\{J_x, J_y, J_z\}$, and the "Bank To Turn" strategy is always used to change

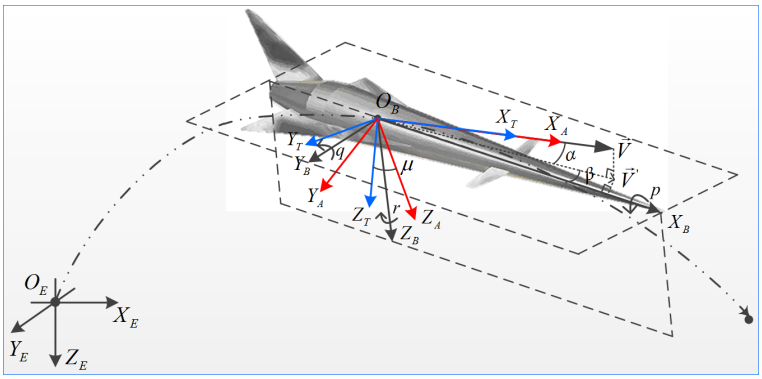


Figure 1: Modeling of the winged-cone HFV

the lateral flight, which means the sideslip angle is always around 0 ($\beta \approx 0$) during the flight.

Under the above reasonable modeling conditions, the nonlinear six-DOF rigid body motion equations of the GHV are derived as follows:

$$
\begin{cases}
\dot{V} = \dfrac{-D - F_{dD}}{m} - g\sin\gamma \\
\dot{\gamma} = \dfrac{L\cos\mu - Y\sin\mu}{mV} - \dfrac{g\cos\gamma}{V} + \dfrac{F_{dL}\cos\mu - F_{dY}\sin\mu}{mV} \\
\dot{\chi} = \dfrac{Y\cos\mu + L\sin\mu + F_{dY}\cos\mu + F_{dL}\sin\mu}{mV\cos\gamma}
\end{cases}
$$

$$
\begin{cases}
J_x\dot{p} = (J_y - J_z)qr + C_1\bar{q}bS + M_{dx} \\
J_y\dot{q} = (J_z - J_x)pr + C_m\bar{q}cS + x_{cg}(D\sin\alpha + L\cos\alpha) + M_{dy} \\
J_z\dot{r} = (J_x - J_y)pq + C_n\bar{q}bS - x_{cg}Y + M_{dz}
\end{cases}
$$

$$
\begin{cases}
\dot{\alpha} = q - \tan\beta(p\cos\alpha + r\sin\alpha) + \dfrac{\bar{G}_\alpha - L + \bar{F}_{d\alpha}}{mV\cos\beta} \\
\dot{\beta} = p\sin\alpha - r\cos\alpha + \dfrac{Y + \bar{G}_\beta + \bar{F}_{d\beta}}{mV} \\
\dot{\mu} = \dfrac{p\cos\alpha + r\sin\alpha}{\cos\beta} + \dfrac{L(\tan\beta + \tan\gamma\sin\mu)}{mV} + \dfrac{Y\tan\gamma\cos\mu + \bar{G}_\mu + \bar{F}_{d\mu}}{mV}
\end{cases}
\tag{1}
$$

Where $V$ is the velocity; $m$ is the mass; $x_{cg}$ is the longitudinal distance from momentum reference to the center of gravity; $b, c, S$ are the main geometric characteristics of the GHV; $\gamma$ is the angle of climb; $\chi$ is the heading an-

gle; $\bar{q} = \rho V^2/2$ is the dynamic pressure, and $\rho$ is the atmos-pheric density. $D, L, Y$ are lift, drag and lateral force, which are respectively determined by $D = C_D\bar{q}S, L = C_L\bar{q}S, Y = C_Y\bar{q}S$ and $C_D, C_L, C_Y, C_l, C_m, C_n$ respectively denote the aerodynamic force and moment coefficients. Besides, $F_{d*}$ and $M_{d*}$ are respectively the external aerodynamic disturbance force and moment, and $\bar{G}, \bar{F}_d$ are equivalent gravity and disturbance forces in TRF.

**Remark 1.** The aerodynamic force and moment coefficients are detailedly given in Ref.[37], which are presented as analytical polynomial functions of the Mach, attitude angles, angular rates, and control surface deflections:

$$\begin{cases} C_D = C_{D\alpha} + C_{D\delta e} + C_{D\delta a} + C_{D\delta r} = f_D\left(Ma, \alpha, \delta_e, \delta_a, \delta_r\right) \\ C_Y = C_{Y\beta} + C_{Y\delta e} + C_{Y\delta a} + C_{Y\delta r} = f_Y\left(Ma, \alpha, \beta, \delta_e, \delta_a, \delta_r\right) \\ C_L = C_{L\alpha} + C_{L\delta e} + C_{L\delta a} = f_L\left(Ma, \alpha, \delta_e, \delta_a\right) \end{cases}$$
$$\begin{cases} C_m = C_{m\alpha} + C_{m\delta e} + C_{m\delta a} + C_{m\delta r} + \dfrac{C_{mq}qc}{2V} = f_m\left(Ma, \alpha, \delta_e, \delta_a, \delta_r, q\right) \\ C_n = C_{n\beta}\beta + C_{n\delta e} + C_{n\delta a} + C_{n\delta r} + \dfrac{(C_{np}p + C_{nr}r)b}{2V} = f_n\left(Ma, \alpha, \beta, \delta_e, \delta_a, \delta_r, p, r\right) \\ C_l = C_{l\beta}\beta + C_{l\delta e} + C_{l\delta a} + C_{l\delta r} + \dfrac{(C_{lp}p + C_{lr}r)b}{2V} = f_l\left(Ma, \alpha, \beta, \delta_e, \delta_a, \delta_r, p, r\right) \end{cases} \tag{2}$$

The nonlinear polynomial functions $f_*$ in the above aerodynamic model have the order up to 7 and the state variables are strongly coupled with each other, which are complex enough to simulate the reality. Therefore this model will be completely adopted to set up later simulation experiments without simplification or decoupling as most studies do.

**Remark 2.** $\delta_e, \delta_a, \delta_r$ respectively denote deflections of the left elevon, right elevon, and rudder, and the saturation nonlinear characteristics of actuators are considered in the simulation, namely, the amplitude and deflection rate of each rudder are limited.

**Remark 3.** The uncertain factors in the dynamical model described in 1) are mainly considered including the structural uncertainty of the GHV ($\Delta m, \Delta\mathbf{J}$), the uncertainty of the atmospheric environment ($\Delta\bar{q}$) and the uncertainty of

aerodynamic coefficients ($\Delta C_D, \Delta C_L, \Delta C_Y, \Delta C_l, \Delta C_m, \Delta C_n$) caused by the modeling deviation of the aerodynamic model 2 and external wind disturbance. The multiplicative perturbed influence factor is used to describe these uncertain parameters, which can be written as

$$\widetilde{\Gamma} = (1 + \Delta\Gamma) * \Gamma \tag{3}$$

where $\Gamma$ denotes a specific parameter among the above uncertain factors, and $\widetilde{\Gamma}$ means the actual value of $\Gamma$.

### *2.2. Basic theory of prescribed performance control*

The so-called prescribed performance means the control performance indices of the system can be directly and quantitatively set in advance and totally guaranteed through proper control. For this purpose, a performance function is firstly defined: a smooth bounded function $\rho(t) : \mathbf{R}^+ \to \mathbf{R}^+$ can be called a performance function, if $\rho(t)$ is positive and decreasing and satisfies $lim_{t\to\infty}\rho(t) = \rho_\infty > 0$. Utilizing the performance function, the control error $e(t)$ can be limited by an inequality constraint:

$$-k_L\rho(t) < e(t) < k_U\rho(t) \quad \begin{cases} k_L = M, k_U = 1 & \text{if } e(0) \geq 0 \\ k_L = 1, k_U = M & \text{if } e(0) \leq 0 \end{cases} \tag{4}$$

where $M \in (0, 1]$ is an adjustable parameter to limit the bound of the overshoot.

Since formula (4) cannot be directly applied to control design, an error transformation function $S(\cdot)$ is introduced to transform the constrained problem into an equivalent unconstrained one:

$$e(t) = \rho(t)S(\varepsilon) \tag{5}$$

To hold the formula (4), $S(\cdot)$ must satisfy the following properties: $S(\cdot)$ is smooth and strictly increasing and defines an onto mapping:

$$\begin{cases} S : (-\infty, \infty) \to (-M, 1) & \text{if } e(0) \geq 0 \\ S : (-\infty, \infty) \to (-1, M) & \text{if } e(0) \leq 0 \end{cases} \tag{6}$$

Then, the virtual error after transformation can be obtained:

$$\varepsilon(t) = S^{-1}\left(\frac{e(t)}{\rho(t)}\right) = T\left(\frac{e(t)}{\rho(t)}\right) \tag{7}$$

where $T(\cdot)$ is the inverse function of $S(\cdot)$.

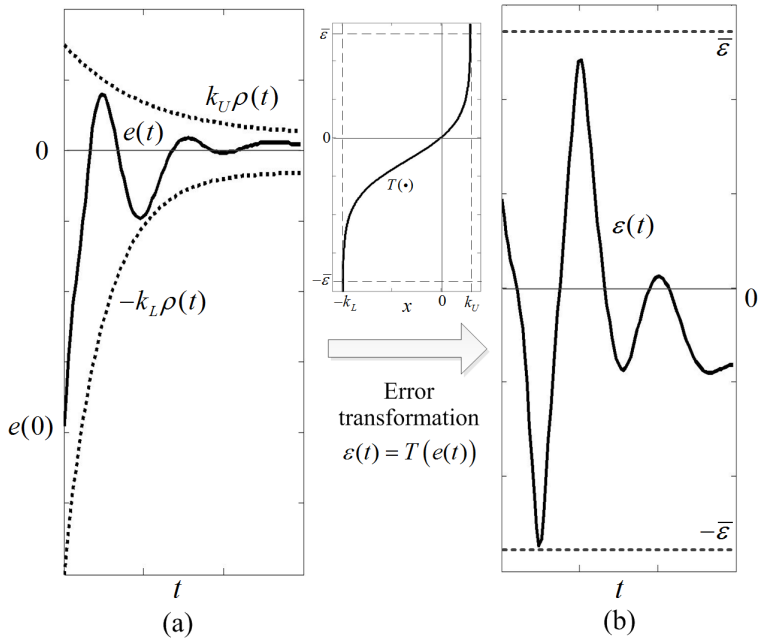


Figure 2: Schematic diagram of the performance constraint and error transformation

The schematic diagram of the control error under performance constraints and its transformation (illustrated by the case of $e(0) \leq 0$) is shown in Fig. 2. From (a), it can be seen that the variation of the control error $e(t)$ is limited to the region surrounded by the performance functions $-\rho(t)$ and $M\rho(t)$. Due to the decreasing property of $\rho(t)$, $e(t)$ will rapidly converge to a small region bounded by $\rho_\infty$ at a convergence rate no less than that of $\rho(t)$, and the maximum overshoot of the error will not be larger than $M\rho(t)$. Therefore, according to the requirements of the transient and steady-state performance of the control error, the comprehensive control performance of the system can be set in advance by selecting appropriate performance function $\rho(t)$ and overshoot index $M$. And (b) illustrated that the actual error $e(t)$ is transformed into virtual

error $\varepsilon(t)$, from which, it can be seen that if $\varepsilon(t)$ is guaranteed to be bounded, the performance constraints set by formula (4) will be satisfied.

**Remark 4.** From Fig. 2, it can be know that the essence of the error transformation is just to change the form of constraint on the error without affecting the setting of the control performance of the system. Therefore, the design goal of the controller is to ensure the boundedness of the virtual error $\varepsilon(t)$.

## 3. Design of prescribed performance controller

### *3.1. Novel performance prescribing scheme*

In most studies related to PPC, the performance prescribing scheme as shown in formula (4) is usually adopted and the corresponding performance function and error transformation function are selected as follows:

$$\rho(t) = (\rho_0 - \rho_\infty)\exp(-lt) + \rho_\infty \tag{8}$$

$$T_1(x(t)) = \frac{1}{2}\ln\left(\frac{k_L k_U + k_U x(t)}{k_L k_U - k_L x(t)}\right) \tag{9}$$

where $x(t) = e(t)/\rho(t)$, and $\rho_0, \rho_\infty$ respectively denote the limitations on the initial error and steady-state error, $l$ denotes the limitation on the convergence rate of the control error.

However, when presetting parameters of the performance indexes in this conventional scheme, there are some inconveniences for practical engineering applications. On the one hand, the limitation on the initial error is not easy to preset unless the initial error of the system is roughly known in advance; on the other hand, since it is usually necessary to take into account some poor conditions in the real operations, the prescribed performance constraint may be inappropriate or too overbroad to achieve the desired effect. Therefore, to improve the conventional performance prescribing scheme, a modified one is introduced by the following three steps.

**Step 1.** Improve the performance function.

Firstly, two basic performance functions that are similar to the conventional one are employed as a rough constraints for the lower and upper bounds of the control error:

$$\begin{cases} g_1(t) = (g_{01} - \zeta/\lambda)\exp(-\lambda t) + \zeta/\lambda \\ g_2(t) = (g_{02} - \xi/\eta)\exp(-\eta t) + \xi/\eta \end{cases} \tag{10}$$

where $g_1(t)$ is used to limit the overshoot of the control error, $g_2(t)$ is used to limit the decreasing of the control error. And $\lambda, \eta, \zeta, \xi, g_{01}$ are arbitrarily adjustable parameters to prescribe desired comprehensive performance: the decreasing rate of the system is not less than $\eta$, the convergence rate of the oscillation (if any) is not less than $\lambda$, the maximum overshoot is not more than $g_{01}$, and the maximum allowable error at the steady state is $min\{\zeta/\lambda, \xi/\eta\}$. Besides, $g_{02}$ is the maximum allowable value of control error or the empirical value of the maximum control error in the actual system. For example, for a flight attitude system, if the control errors of attitude angles go beyond $5^\circ$ or $10^\circ$, the control can be considered totally invalid.

Secondly, a variable nonlinear scaling factor $s_c$ named "adaptively alterable constraint (AAC) factor" in this paper is defined to construct the precise performance functions $h_1(t), h_2(t)$:

$$h_1(t) = -s_c g_1(t); h_2(t) = s_c g_2(t) \quad \begin{cases} s_c = \tanh(e_0/a) & e_0 > z_0 \\ s_c = \tanh(z_0/a) & e_0 \le z_0 \end{cases} \tag{11}$$

where $e_0$ is the initial error measured while the control system starts running, $z_0$ is a threshold of the initial error and determines the minimum value of the AAC factor, normally, $z_0 \ge min\{\zeta/\lambda, \xi/\eta\}$. And $a \in \mathbf{R}^+$ is used to adjust the sensitivity of the AAC factor's changing.

Finally, the performance constraint for the lower and upper bounds of the control error can be set by $\rho_L(t)$ and $\rho_U(t)$, which is

$$\begin{aligned} &\rho_L(t) < e(t) < \rho_U(t) \\ &\rho_L(t) = \min\{h_1(t), h_2(t)\}; \rho_U(t) = \max\{h_1(t), h_2(t)\} \end{aligned} \tag{12}$$

In this new scheme, the improvement of the performance function is not as complicated as in Ref.[33] or Ref.[35], but the meaning of each parameter is

more clear, the setting of the performance constraints is more flexible,and there is just one parameter ($a$) needs to be adjusted according to the specific system.

**Remark 5.** The AAC factor plays an important role in this novel scheme, whose effects can be interpreted as follows:

- The sign of initial error can be indirectly reflected by the tanh function, thereby avoiding to consider the positive and negative cases separately like the conventional method;
- The actual performance constraints affected by the actual initial errors are variable between a preset zone, namely, when the initial error is small, the performance constraint will be correspondingly strict so that the control accuracy can be further improved. In contrast, the conventional performance prescribing is not flexible enough for practical applications because of its fixed parameters. An example illustration for the actual performance constraints of different initial errors ($e_0 = 4, 1, 0.5$) using the novel performance prescribing scheme is shown in Fig. 3, in which $L_{e0*}$ and $U_{e0*}$ respectively denote the lower and upper bounds of the actual performance constraints.
- Because of the variability of constraints, it is unnecessary to know the exact initial error in advance like the conventional method, a rough possible upper bound of the initial error ($g_{02}$) that is easy to be found in a real system is enough for the implementation of the new method.

**Step 2.** Introduce a performance constraint resetting (PCR) mechanism.

In most studies related to PPC, the performance trans-gression problem is rarely considered. However, when some unexpected conditions happen in the actual system, such as the system in the steady-state is suddenly subjected to large external disturbances, or the system reference command is abruptly changed, or the system fails unexpectedly, etc., the control error of the system may exceed the limit of the prescribed constraint. If no measures are taken in time

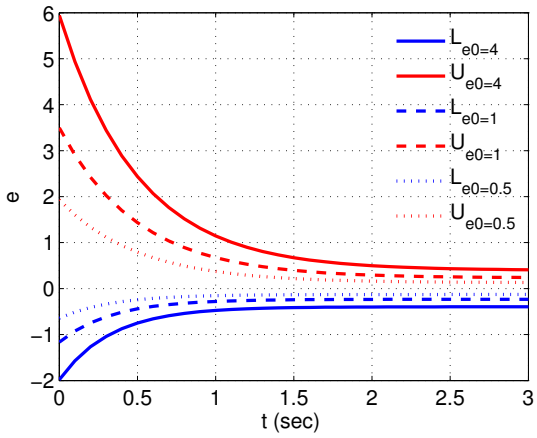


Figure 3: An illustration of the the novel performance prescribing scheme

for this problem, mistakes will occur in the calculation of the control error transformation, which probably cause the divergence of the system. Aiming at this potential pitfall, a performance constraint resetting mechanism is proposed.

The concept of "convergence period of the control error" is firstly defined as a period of time during which the control error under the restraint of performance constraints gradually converges from the initial state until the error exceeds the current set constraint due to some factors. Therefore, it can be known that the entire running time of the system consists of one or more convergence periods. The so-called PCR mechanism means the process of ending the current convergence period and starting a new one, namely, when the control error of the abnormal system exceeds the constraint boundary, it is considered that the previous preset constraint no longer matches the system and needs to be reset to force the control error to converge back to a new error boundary.

Based on the novel performance functions described in 1, the resetting process of the constraint mainly includes the zeroing of convergence counting-time ($t_r = 0$), the updating of the adaptively alterable constraint factor by finding the initial maximum error for the new convergence period, and the setting of new performance boundaries.

**Step 3.** Modify the error transformation function

As for the new performance constraint shown in formula (12), the error transformation function can be modified as:

$$\begin{aligned} \varepsilon(t) =& T_2\left(e(t), \rho_U(t), \rho_L(t)\right) = \ln\left(\frac{\kappa}{1-\kappa}\right) \\ \kappa =& \left(e(t)-\rho_L(t)\right) / \left(\rho_U(t)-\rho_L(t)\right) \end{aligned} \tag{13}$$

and the time derivative of the above virtual error $\varepsilon(t)$ can be derived as:

$$\begin{aligned} \dot{\varepsilon}(t) =& \frac{1-\kappa}{\kappa}\left(\frac{e(t)-\rho_L(t)}{\rho_U(t)-\rho_L(t)}\right)' \\ =& \frac{1-\kappa}{\kappa}\left(\frac{\dot{e}}{\rho_U-\rho_L} - \frac{e\left(\rho_U'-\rho_L'\right)}{\left(\rho_U-\rho_L\right)^2} + \frac{\rho_L\rho_U'-\rho_U\rho_L'}{\left(\rho_U-\rho_L\right)^2}\right) \\ =& \frac{1-\kappa}{\kappa}\operatorname{sign}\left(e_0\right)\left(\frac{\dot{e}}{s_c\left(g_2+g_1\right)} - \frac{e^*\left(g_2'+g_1'\right)}{s_c\left(g_2+g_1\right)^2} + \frac{\left(g_2g_1'-g_1g_2'\right)}{\left(g_2+g_1\right)^2}\right) \\ =& \bar{T}_{d2}(e,t)\dot{e}(t) + \bar{T}_{c2}(e,t) \end{aligned} \tag{14}$$

where $g_n = (1-\kappa)/\kappa; g_o = g_1+g_2; g_p = g_2g_1'-g_1g_2', \bar{T}_{d2}(t) = \frac{\operatorname{sign}(e_0)g_n}{s_c g_o}; \bar{T}_{c2}(e,t) = \frac{\operatorname{sign}(e_0)g_n}{g_o^2}\left(-\frac{g_0'}{s_c}e + g_p\right)$

Investigated the inverse transformation of formula (13):

$$\kappa(t) = \frac{\exp(\varepsilon(t))}{1+\exp(\varepsilon(t))} \tag{15}$$

from which, it can be known if the virtual error is bounded, that is, there is a bounded constant $\bar{\varepsilon} \in \mathbf{R}^+$ such that $|\varepsilon(t)| \leq \bar{\varepsilon}$, then we have:

$$0 < \frac{\exp\left(-\bar{\varepsilon}\right)}{1+\exp\left(-\bar{\varepsilon}\right)} < \kappa(t) < \frac{\exp\left(\bar{\varepsilon}\right)}{1+\exp\left(\bar{\varepsilon}\right)} < 1 \tag{16}$$

that is,

$$0 < \frac{e(t)-\rho_L(t)}{\rho_U(t)-\rho_L(t)} < 1 \Rightarrow \rho_L(t) < e(t) < \rho_U(t) \tag{17}$$

which proves that under the action of the selected error transformation function, the actual control error of the system will meet the prescribed performance as long as the transformed virtual error is guaranteed to be bounded.

Above all of these three steps, the specific implementation process of the novel performance prescribing scheme can be expressed as a flow chart shown in Fig. 4.

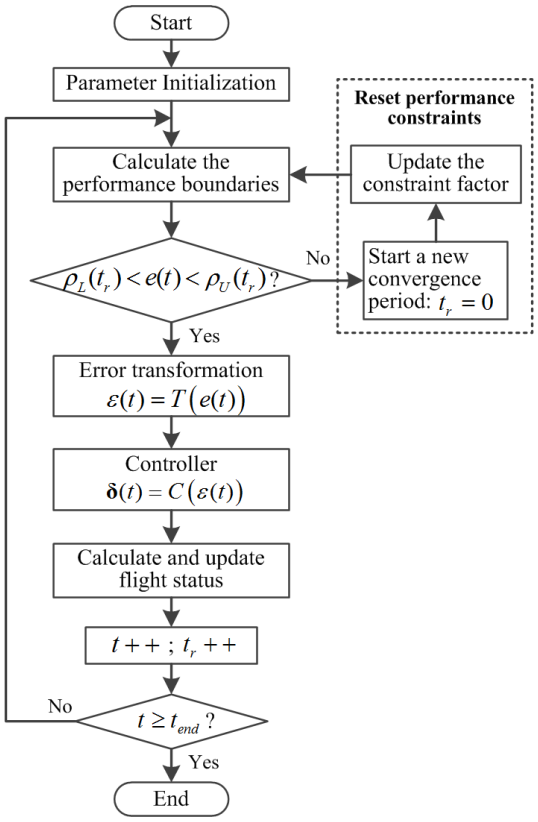


Figure 4: Flow chart of the performance constraint resetting strategy

### *3.2. Controller design and stability analysis*

To design a prescribed performance controller for the attitude tracking control of GHV, the dynamical model (1) is firstly simplified to obtain its affine nonlinear form:

$$\begin{aligned} \dot{\Theta} =& \mathbf{g}_s \boldsymbol{\omega} + \boldsymbol{\Delta}_s \\ \dot{\boldsymbol{\omega}} =& \mathbf{g}_f U + \mathbf{f}_f(\boldsymbol{\omega}) + \boldsymbol{\Delta}_f \end{aligned} \tag{18}$$

where $U = [\delta_e, \delta_a, \delta_r]^T$ is the control surface vector; $\mathbf{g}_s, \mathbf{g}_f$ are the state matrixes of the angle control system and angular rate control system, respectively; $\mathbf{f}_f(\boldsymbol{\omega}) = [f_q, f_r, f_p]^T$ is the vector function of attitude angular rate.The detailed expressions of these variables are given in the "Appendix". $\boldsymbol{\Delta}_s =$

$[\Delta_{s1}, \Delta_{s2}, \Delta_{s3}]^T, \boldsymbol{\Delta}_f = [\Delta_{f1}, \Delta_{f2}, \Delta_{f3}]^T$ are the total equivalent unknown deviations including modeling errors, parameter uncertainties and external disturbances.

**Assumption 1.** For the time-varying total equivalent unknown devia-tions, there exists upper bounds in a real system. Assume the estimated upper bounds for the three control channels are respectively $\boldsymbol{\Delta}_{sE} = [\Delta_{sE1}, \Delta_{sE2}, \Delta_{sE3}]^T, \boldsymbol{\Delta}_{fE} = [\Delta_{fE1}, \Delta_{fE2}, \Delta_{fE3}]^T$, that is $|\Delta_{s*}| \leq |\Delta_{sE*}|$.

**Assumption 2.** The attitude angle reference commands $\boldsymbol{\Theta}_d = [\alpha_d, \beta_d, \mu_d]^T$ and the desired virtual angular rate $\boldsymbol{\omega}_d = [e_q, e_r, e_p]^T$ in two control loops are both second-order differentiable continuous signals. Thus the tracking error vectors can be obtained as follows:

$$\mathbf{e}_\Theta = \boldsymbol{\Theta} - \boldsymbol{\Theta}_d = [e_\alpha, e_\beta, e_\mu]^T; \quad \mathbf{e}_\omega = \boldsymbol{\omega} - \boldsymbol{\omega}_d = [q_d, r_d, p_d]^T \tag{19}$$

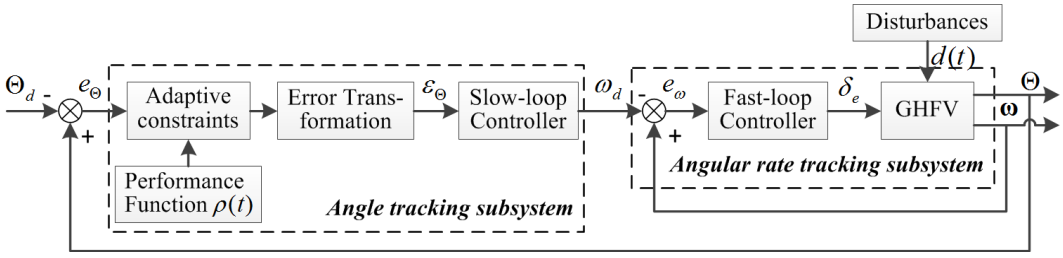


Figure 5: Architecture of the dual-loop control based on PPC theory

Based on the proposed novel performance prescribing scheme, a dual-loop control architecture as shown in Fig. 5 is designed. In the inner loop, a valid controller is firstly needed for the angular rate error $\mathbf{e}_\omega$ to ensure its faster convergence. And the prescribed performance constraint is introduced into the outer loop to guarantee a better comprehensive tracking control performance, in which process, the performance constraints are adaptivly set and the actual angle control errors $\mathbf{e}_\Theta$ are transformed into the virtual errors $\varepsilon_\Theta$, whereafter a outer-loop controller can be designed for the virtual error to ensure its boundedness.

It is obvious that the design of these two controllers can be flexible as long as the boundedness of the virtual error can be ensured by outer-loop controller and the stability of the angular rate taracking subsystem can be ensured by inner-loop controller, for example, the common PID control or widely used backstepping control can be feasible. For further verification, the well-developed sliding mode control method is selected to design simple enough non-linear robust controllers.

**Step 1.** The angle control in the outer loop

According to the error transformation formula (13), the virtual control error can be calculated:

$$\boldsymbol{\varepsilon}_{\Theta} = T\left(\mathbf{e}_{\Theta}\right) = \left[\varepsilon_{\alpha}, \varepsilon_{\beta}, \varepsilon_{\mu}\right]^{T} \tag{20}$$

For the virtual control error $\boldsymbol{\varepsilon}_{\Theta}$, define an integral sliding mode surface as follows:

$$\boldsymbol{\sigma}_{I}(t) = \boldsymbol{\varepsilon}_{\Theta}(t) + \mathbf{c}_{o} \int_{0}^{t} \boldsymbol{\varepsilon}_{\Theta}(t) dt \tag{21}$$

where $\mathbf{c}_{o} = diag\{c_{o1}, c_{o2}, c_{o3}\}, c_{o*} > 0$ is the integral coefficients. When the system reaches the sliding mode surface, $\sigma(t) = 0$ will be satisfied, and the virtual error $\boldsymbol{\varepsilon}_{\Theta}$ will exponentially converge, so that its boundedness can be guaranteed.

In order to improve the dynamic quality of the system, the exponential approach law is employed to design the controller [38], which is:

$$\dot{\boldsymbol{\sigma}}_{o}(t) = -\mathbf{k}_{1}\,\mathrm{sign}(\boldsymbol{\sigma}_{\boldsymbol{o}}) - \mathbf{k}_{2}\boldsymbol{\sigma}_{\boldsymbol{o}} \tag{22}$$

where $\mathbf{k}_{1} = \mathrm{diag}\{k_{11}, k_{12}, k_{13}\}, \mathbf{k}_{2} = \mathrm{diag}\{k_{21}, k_{22}, k_{23}\}$ are coefficients that determine the rate of convergence ($k_{*} > 0$).

According to the affine nonlinear model of the GHV's dynamics (2) and formula (13), differentiating equation (21) yields

$$\begin{aligned} \dot{\boldsymbol{\sigma}}_{o}(t) &= \dot{\boldsymbol{\varepsilon}}_{\Theta}(t) + \mathbf{c}_{o}\boldsymbol{\varepsilon}(t) \\ &= \bar{\mathbf{T}}_{d}(\mathbf{e}_{\Theta})\left(\mathbf{g}_{s}\boldsymbol{\omega}_{v} + \boldsymbol{\Delta}_{s} - \dot{\boldsymbol{\Theta}}_{d}\right) + \bar{T}_{c}(\mathbf{e}_{\Theta}) + \mathbf{c}_{o}T(\mathbf{e}_{\Theta}) \end{aligned} \tag{23}$$

where $\bar{\mathbf{T}}_d(\mathbf{e}_\Theta) = \mathrm{diag}\{\bar{T}_d(e_\alpha), \bar{T}_d(e_\beta), \bar{T}_d(e_\mu)\}$. Thus, the angle tracking controller can be derived as follows:

$$\boldsymbol{\omega}_v = \left(\bar{\mathbf{T}}_d(\mathbf{e}_\Theta)\boldsymbol{g}_s\right)^{-1}\Big[\bar{\mathbf{T}}_d(\mathbf{e}_\Theta)*\left(\dot{\boldsymbol{\Theta}}_d - \boldsymbol{\Delta}_{sE}\right) - \bar{T}_c(\mathbf{e}_\Theta) - \mathbf{c}_o T(\mathbf{e}_\Theta) - \mathbf{k}_1\,\mathrm{sign}(\boldsymbol{\sigma}_o) - \mathbf{k}_2\boldsymbol{\sigma}_o\Big] \tag{24}$$

where $\boldsymbol{\Delta}_{sE}$=$[\Delta_{sE1}, \Delta_{sE2}, \Delta_{sE3}]^T \cdot \mathrm{sign}(\boldsymbol{\sigma}_o)$.

**Step 2.** The angular rate control in the inner loop

In the same way, another integral sliding mode controller is designed for the angular rate control, whose expectation is the output of the outer loop, that is $\boldsymbol{\omega}_d = \boldsymbol{\omega}_v$. The corresponding integral sliding mode surface and its derivative can be similarly defined as following:

$$\begin{aligned} \boldsymbol{\sigma}_i(t) &= \mathbf{e}_\omega(t) + \mathbf{c}_i \int_0^t \mathbf{e}_\omega(t)dt \\ \dot{\boldsymbol{\sigma}}_i(t) &= (\dot{\boldsymbol{\omega}} - \dot{\boldsymbol{\omega}}_d) + \mathbf{c}_i\mathbf{e}_\omega(t) = \boldsymbol{g}_f U + \mathbf{f}_f(\boldsymbol{\omega}) + \boldsymbol{\Delta}_f - \dot{\boldsymbol{\omega}}_d + \mathbf{c}_i\mathbf{e}_\omega(t) \end{aligned} \tag{25}$$

And based on the exponential approach law, the inner loop controller can be designed:

$$U = \boldsymbol{g}_f^{-1}(\dot{\boldsymbol{\omega}}_d - \mathbf{f}_f(\boldsymbol{\omega}) - \mathbf{c}_i\mathbf{e}_\omega(t) - \boldsymbol{\Delta}_{fE} - \mathbf{k}_3\,\mathrm{sign}(\boldsymbol{\sigma_i}) - \mathbf{k}_4\boldsymbol{\sigma_i}) \tag{26}$$

**Remark 6.** To further reduce the influence of sliding mode chattering caused by discontinuity of sign function, the tanh function can be used to replace the sign function in the above formulas.

**Step 3.** Stability analysis

To analyze the stability of the outer loop subsystem, define a Lyapunov function $V = \boldsymbol{\sigma}_o^T\boldsymbol{\sigma}_o/2$, and its derivative can be derived:

$$\dot{V} = \boldsymbol{\sigma}_o^T\dot{\boldsymbol{\sigma}}_o = \boldsymbol{\sigma}_o^T\left(-\mathbf{k}_1\,\mathrm{sign}(\boldsymbol{\sigma}_o) - \mathbf{k}_2\boldsymbol{\sigma}_o + \bar{\mathbf{T}}_d(\mathbf{e}_\Theta)\left(\boldsymbol{\Delta}_s - \boldsymbol{\Delta}_{sE}\right)\right) \tag{27}$$

Analyzing the above equation, it can be known that if $\bar{T}_d(e) \geq 0$ is true, $\dot{V} < 0$ will be always held regardless of the positive and negative of the sliding mode variable $\sigma_o$, which means that the system will be asymptotically stable. And

investigating the error transformation formula (13), it can be found that as long as the control error $e(t)$ is within the prescribed constraint bounds, the above conditions can be satisfied. Thus the performance constraint resetting mechanism described in the previous subsection can effectively avoid the possibility of the transgression of control error and enhance the stability of the system.

The asymptotic stability of the inner loop subsystem can be easily proved by a similar Lyapunov function, and it will not be repeated in detail.

## 4. Simulation Results

To validate the feasibility and superiority of the improved PPC scheme, a numerical simulation platform is established based on the nonlinear six-DOF attitude dynamic model of GHV, in which the fourth-order Runge-Kutta method is employed, and the step size is set to 0.005 sec. Besides, for the selected reentry flight phase, the main model parameters are listed in Table 1, the aerodynamic coefficients are calculated according to Ref.[37], and the initial trim conditions of the simulation are set as follows: $V_0$=4590$m/s$, $h_0$=33000$m$, $\alpha_0$=$\beta_0$=$\mu_0$ = 0, $q$=$p$=$r$=0. In addition, as stated in Remark 2, the saturation nonlinear characteristics of actuators are taken into account in the simulation: the amplitude of each rudder is limited upto $\pm 20^\circ$ and the deflection rate of each rudder is limited upto $10 rad/s$.

Based on the above simulation conditions, two simulation cases are carried out to fully demonstrate the proposed new scheme: the pitch maneuver control using step command and the attitude tracking of three control channels using a set of reentry flight commands. Besides, a first-order filter with the time constant of 0.3 sec is added after the input of angle commands to avoid its discontinuousness.

### *4.1. Pitch maneuver control*

For the pitch control subsystem without any disturbances, a step command with the amplitude of 5 degrees is firstly applied at the time of 2 sec. The control effect of the system using the novel prescribed performance control (NPPC)

Table I: The main model parameters of GHV

| Item | Symbol | Value | Unit |
|---|---|---|---|
| Mass | $m_0$ | 63500 | Kg |
| Chord | $c$ | 24.384 | m |
| Span | $b$ | 18.288 | m |
| Reference area | $S$ | 334.73 | $m^2$ |
| Center of gravity | $x_{cg}$ | 4.4668 | m |
| Moment of inertia | $J_y, J_z$ | 6101181 | $Kg{\cdot}m^2$ |
| | $J_x$ | 637234 | $Kg{\cdot}m^2$ |

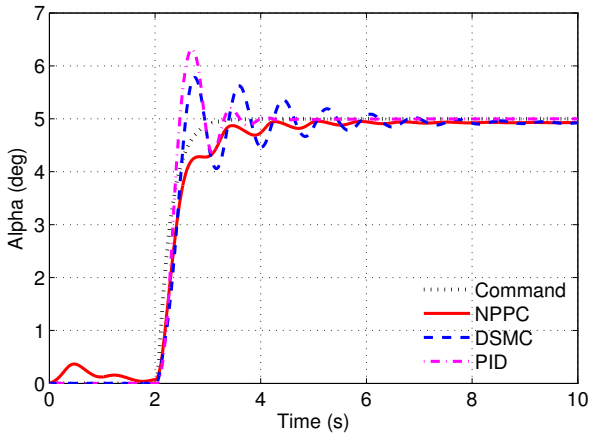


Figure 6: Step responses of the pitch control

are shown in Fig. 6 and Fig. 7, in which, a double-loop integral sliding mode controller (DSMC) with the same inner loop control parameters as NPPC and a classical PID controller that have been finely tuned are respectively employed into the system for comparison. From the two figures, it can be seen that both PID and DSMC can achieve good control performance, with high control accuracy and fast response speed, but the overshoot of PID is larger, and the error convergence of DSMC is slower. In contrast, NPPC shows better comprehensive control performance with a similar response speed and control accuracy but

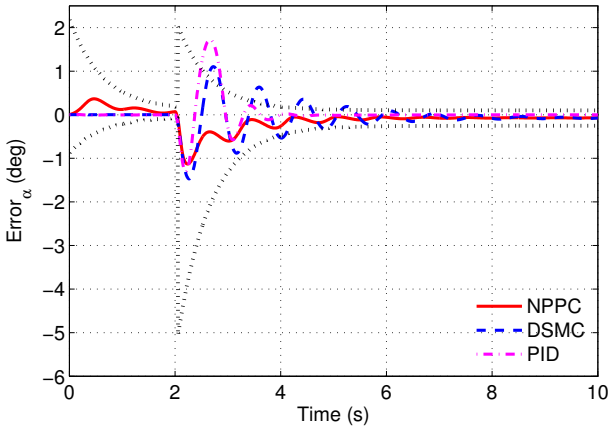


Figure 7: Pitch Control errors in the step test

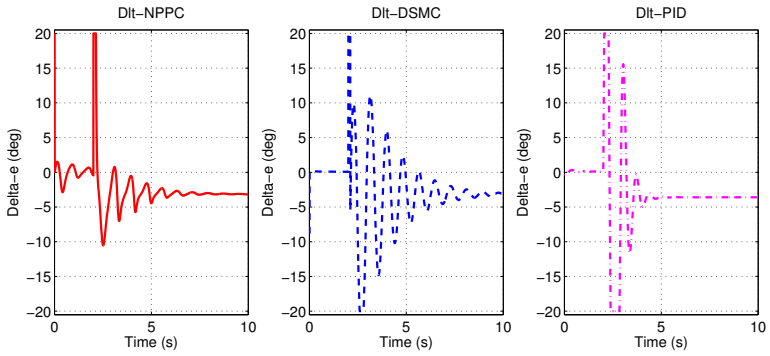


Figure 8: Comparison of the elevator deflections in the step test

non-overshooting and faster convergence. And the change of the control error is within the set performance constraints all the time, which is the result of conducting the prescribed performance scheme.

Besides, the comparison of elevator deflections of the system using these three methods is shown in Fig. 8, and the transformed virtual control error of NPPC is shown in Fig. 9. It can be seen that the elevator deflections are realizable for the real system, and the virtual error of NPPC is always convergent and bounded, which indicates the effectiveness of the designed controller.

Subsequently, the torque shocks of different amplitudes are enforced to the

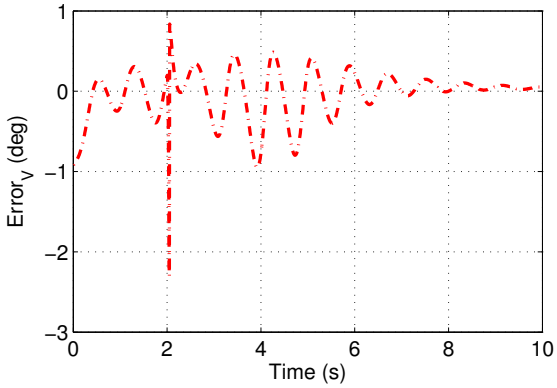


Figure 9: The transformed virtual control error of NPPC in the step test

pitch channel at the time of 6 sec to simulate the gust interference that may be encountered in the flight. The control performance of the system using the conventional PPC presented in Ref.[29] is shown in Fig. 10, and that of the NPPC is shown in Fig. 11. As can be seen by comparing the conventional and novel methods, to deal with interference, the conventional method often needs to set a wider performance boundary, that is, by sacrificing the control performance in exchange for stronger robustness, even so, the conventional method is still difficult to resist large external disturbance, which means when the disturbance reaches a certain level, the system will be at risk of instability. While the proposed novel method can adaptively set performance boundaries according to the real-time control error of the system, which makes it possible for the system to readjust the performance constraints and force the error to converge again. Therefore, the new method can better deal with external disturbances, especially the large ones, which is a significant advantage of the new method.

### *4.2. Attitude tracking for the reentry flight*

To further verify the performance of the proposed NPPC on the attitude tracking control of the GHV, a three-channel attitude tracking control simulation is carried out for the reentry flight with large aerodynamic interference. A set of flight control commands as shown in Fig. 12 (a) is simply designed,

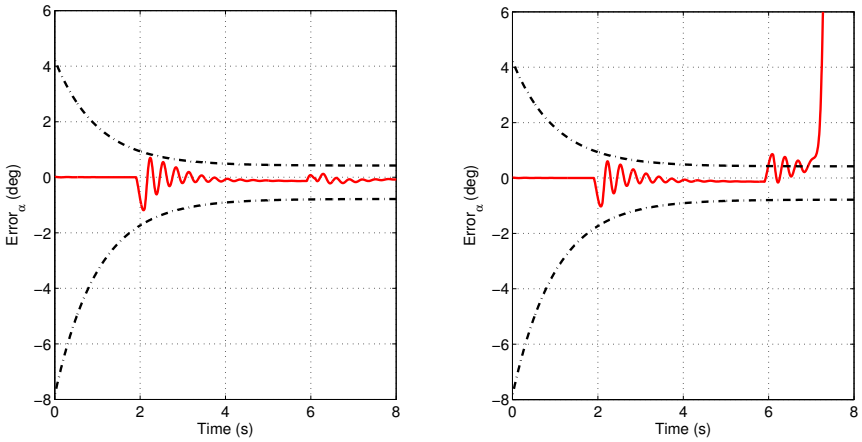


(a) The small disturbance case (b) The large disturbance case

Figure 10: Control errors of the conventional method under external disturbances

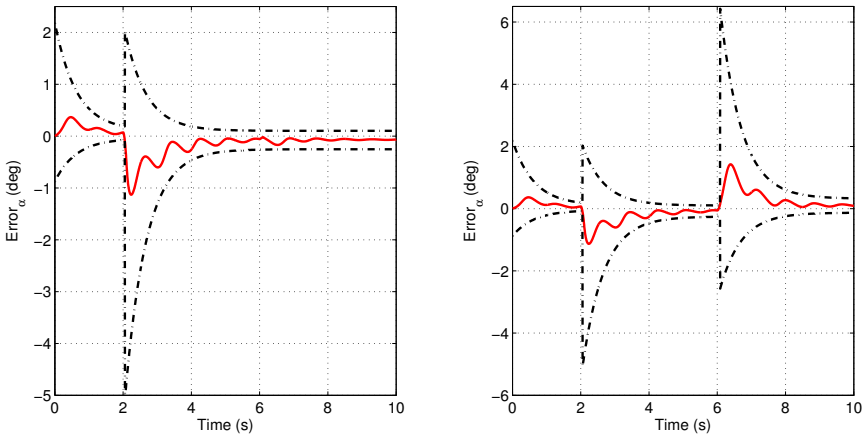


(a) The small disturbance case (b) The large disturbance case

Figure 11: Control errors of the novel method under external disturbances

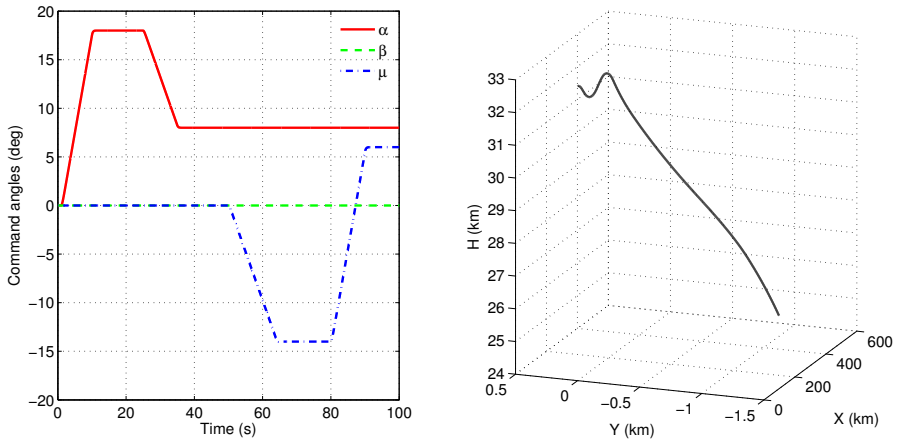


(a) Angle commands (b) Nominal trajectory

Figure 12: The command and trajectory for a reentry flight

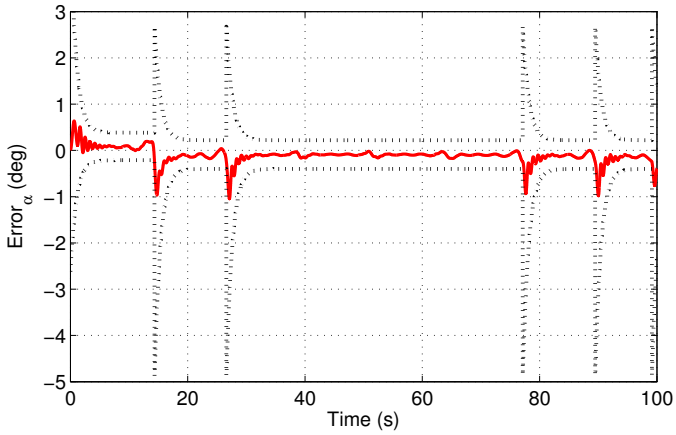


Figure 13: The tracking control error of pitch channel during reentry flight

and the corresponding nominal trajectory is shown in Fig. 12(b), which is a typical reentry flight with a height drop of $8km$ and a lateral movement of $1km$ in 100 sec.

Besides, it is assumed that during the whole flight, the structural parameters of the GHV have an uncertain deviation of 20%, that is $\tilde{m}_0 = m_0 * (1 + 0.2 *$

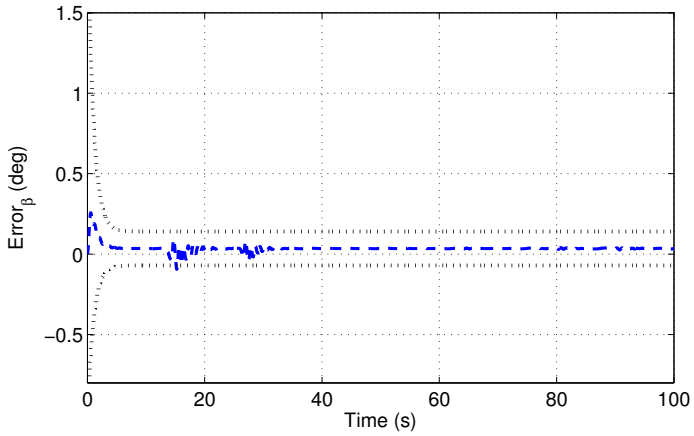


Figure 14: The tracking control error of yaw channel during reentry flight

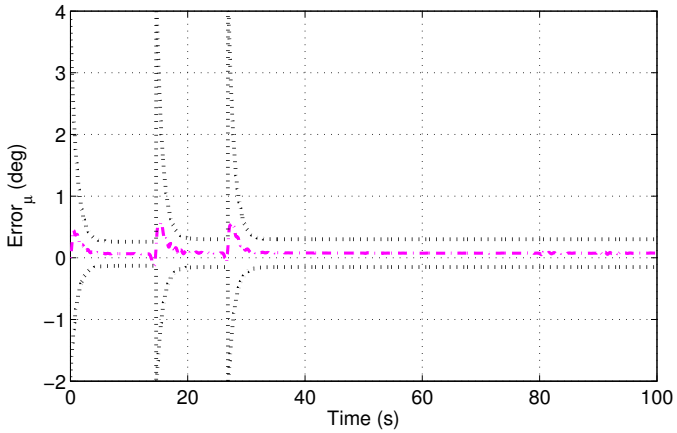


Figure 15: The tracking control error of roll channel during reentry flight

$rand(\cdot)), \tilde{\mathbf{J}} = \mathbf{J} * (1 + 0.2 * rand(\cdot))$ and the aerodynamic coefficients are also disturbed by uncertainty:

$$\begin{cases} \tilde{C}_D = C_D * (1 + \Delta(0)) \\ \tilde{C}_Y = C_Y * (1 + \Delta(0.8\pi)) \\ \tilde{C}_L = C_L * (1 + \Delta(1.6\pi)) \end{cases} \quad \begin{cases} \tilde{C}_l = C_l * (1 + \Delta(0.4\pi)) \\ \tilde{C}_m = C_m * (1 + \Delta(1.2\pi)) \\ \tilde{C}_n = C_n * (1 + \Delta(2\pi)) \end{cases} \tag{28}$$

where $\Delta(x) = 0.1 * [\sin(0.5t + x) + \sin(t + x) + \sin(1.5t + x) + \sin(2t + x)]$.

The three-channel attitude tracking control error curves are obtained and

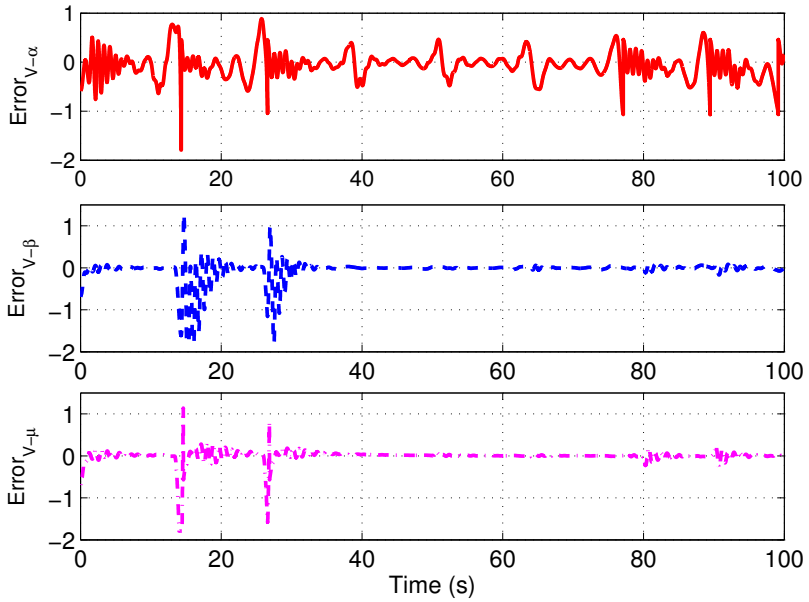


Figure 16: The virtual control errors during reentry flight

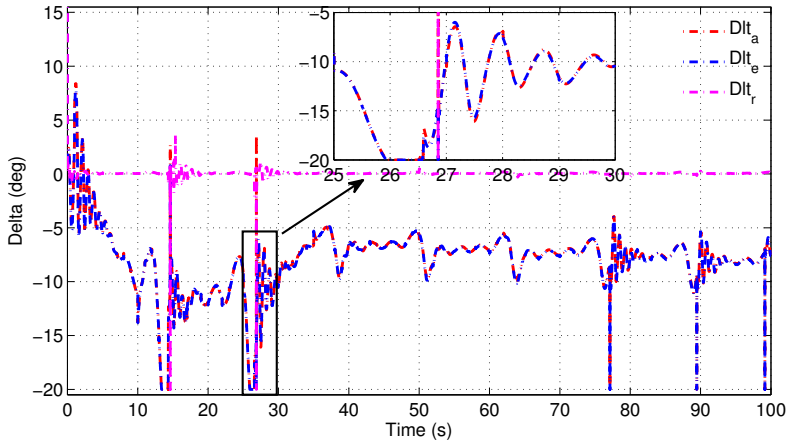


Figure 17: The actual control surface deflections during reentry flight

respectively shown in Figs. 13-15, the corresponding virtual control error curves are shown in Fig. 16, and the actual control surface deflection curves are shown

in Fig. 17. It can be seen that under the intense influence of a large amount of uncertainty, the system using the NPPC method can always track the command signal stably and achieve excellent control performance: the control errors are always within the set performance boundaries, and the virtual errors are always bounded and converge to near 0, which makes the convergence rate, control accuracy, and overshoot of the actual control error guaranteed with the prescribed performance.

## 5. Conclusion

In this paper, a novel prescribed performance control scheme is improved and applied to the attitude tracking control of the hypersonic vehicle. The nonlinear dynamic modeling for the reentry flight and the basic theory of prescribed performance control are first introduced. Then, the improvements on the conventional prescribed performance control are detailedly described, including a novel performance constraint scheme with adaptively alterable constraint and a performance constraint resetting mechanism. Afterward, a simple dual-loop integral sliding mode controller is designed based on the improved new scheme. Numerical simulations in both pitch maneuver control and three-channel attitude tracking control cases are finally conducted to verify the effectiveness of the proposed method.

The improved method can achieve better comprehensive control performance and has a strong anti-disturbance ability, which is more practical than the conventional method. However, to fully extend the prescribed performance control method to the real engineering applications, other issues need to be further considered, such as the actuator rate saturation, the weak model dependent control design, and so on.

## Acknowledgements

This work was supported by the National Natural Science Foundation of China under Grant ***.

## References


[1] Guan Z, Ma Y, Zheng Z, Guo N. Prescribed performance control for automatic carrier landing with disturbance. Nonlinear Dyn 2018;94(2):1335–49. doi:10.1007/s11071-018-4427-3.

[2] Zhang C, Ma G, Sun Y, Li C. Simple model-free attitude control design for flexible spacecraft with prescribed performance. Proc Inst Mech Eng Part G-J Aerosp Eng 2019;233(8):2760–71. doi:10.1177/0954410018786085; publisher: SAGE Publications Sage UK: London, England.

[3] Yang GH, Lum KY. Gain-scheduled flight control via state feedback. In: Proceedings of the 2003 American Control Conference, 2003.; vol. 4. 2003, p. 3484–9. doi:10.1109/ACC.2003.1244072; iSSN: 0743-1619.

[4] Tao X, Li N, Li S. Multiple model predictive control for large envelope flight of hypersonic vehicle systems. Inf Sci 2016;328:115–26. doi:10.1016/j.ins.2015.08.033.

[5] Chen W. Nonlinear disturbance observer-enhanced dynamic inversion control of missiles. J Guid Control Dyn 2003;26(1):161–6. doi:10.2514/2.5027.

[6] Ma G, Chen C, Lyu Y, Guo Y. Adaptive backstepping-based neural network control for hypersonic reentry vehicle with input constraints. IEEE Access 2018;6:1954–66. doi:10.1109/ACCESS.2017.2780994.

[7] Hu Q, Meng Y. Adaptive backstepping control for air-breathing hypersonic vehicle with actuator dynamics. Aerosp Sci Technol 2017;67:412–21. doi:10.1016/j.ast.2017.04.022.

[8] Wang Q, Stengel RF. Robust nonlinear control of a hypersonic aircraft. J Guid Control Dyn 2000;23(4):577–85.

[9] Yin X, Li X, Liu L, Wang Y, Wei X. A probabilistic robust mixed h-2/h-infinity fuzzy control method for hypersonic vehicles based on reli-

ability theory. Int J Adv Robot Syst 2018;15(1):1–15. doi:10.1177/1729881417754153.

[10] An B, Wang B, Wang Y, Liu L. Adaptive terminal sliding mode control for reentry vehicle based on nonlinear disturbance observer. IEEE Access 2019;7:154502–1. doi:10.1109/ACCESS.2019.2948963; conference Name: IEEE Access.

[11] Hu X, Wu L, hu C, Gao H. Adaptive fuzzy integral sliding mode control for flexible air-breathing hypersonic vehicles subject to input nonlinearity. J Aerosp Eng 2013;26:721–34. doi:10.1061/(ASCE)AS.1943-5525.0000193.

[12] Yin X, Wang B, Liu L, Wang Y. Disturbance observer-based gain adaptation high-order sliding mode control of hypersonic vehicles. Aerosp Sci Technol 2019;89:19–30. doi:10.1016/j.ast.2019.03.030.

[13] Bu XW, Wu XY, Chen YX, Bai RY. Design of a class of new nonlinear disturbance observers based on tracking differentiators for uncertain dynamic systems. Int J Control Autom Syst 2015;13(3):595–602. doi:10.1007/s12555-014-0173-6.

[14] Bu X, Wu X, Wei D, Huang J. Neural-approximation-based robust adaptive control of flexible air-breathing hypersonic vehicles with parametric uncertainties and control input constraints. Inf Sci 2016;346-347:29–43. doi:10.1016/j.ins.2016.01.093.

[15] Xia R, Chen M, Wu Q, Wang Y. Neural network based integral sliding mode optimal flight control of near space hypersonic vehicle. Neurocomputing 2020;379:41–52. doi:10.1016/j.neucom.2019.10.038.

[16] Chen B, Tong S, Liu X. Fuzzy approximate disturbance decoupling of MIMO nonlinear systems by backstepping approach. Fuzzy Sets Syst 2007;158(10):1097–125. doi:10.1016/j.fss.2006.12.012.

[17] Mao Q, Dou L, Zong Q, Ding Z. Attitude controller design for reusable launch vehicles during reentry phase via compound adaptive fuzzy H-

infinity control. Aerosp Sci Technol 2018;72:36–48. doi:10.1016/j.ast.2017.10.012.

[18] Sun H, Li S, Sun C. Finite time integral sliding mode control of hypersonic vehicles. Nonlinear Dyn 2013;73(1):229–44. doi:10.1007/s11071-013-0780-4.

[19] Geng J, Sheng Y, Liu X. Finite-time sliding mode attitude control for a reentry vehicle with blended aerodynamic surfaces and a reaction control system. Chin J Aeronaut 2014;27(4):964 –76. doi:10.1016/j.cja.2014.03.013.

[20] ZHANG L, WEI C, WU R, CUI N. Fixed-time adaptive model reference sliding mode control for an air-to-ground missile. Chin J Aeronaut 2019;32(5):1268 –80. doi:10.1016/j.cja.2018.10.008.

[21] Miller DE, Davison E. An adaptive controller which provides an arbitrarily good transient and steady-state response. IEEE Trans Autom Control 1991;36(1):68–81. doi:10.1109/9.62269.

[22] Ilchmann A, Ryan EP, Trenn S. Tracking control: performance funnels and prescribed transient behaviour. Syst Control Lett 2005;54(7):655–70. doi:10.1016/j.sysconle.2004.11.005.

[23] Bechlioulis CP, Rovithakis GA. Adaptive control with guaranteed transient and steady state tracking error bounds for strict feedback systems. Automatica 2009;45(2):532–8. doi:10.1016/j.automatica.2008.08.012.

[24] Bechlioulis CP, Rovithakis GA. Prescribed performance adaptive control for multi-input multi-output affine in the control nonlinear systems. IEEE Trans Autom Control 2010;55(5):1220–6. doi:10.1109/TAC.2010.2042508.

[25] Wang M, Yang A. Dynamic learning from adaptive neural control of robot manipulators with prescribed performance. IEEE Trans Syst Man Cybern -Syst 2017;47(8):2244–55. doi:10.1109/TSMC.2016.2645942.

[26] Jing C, Xu H, Niu X. Adaptive sliding mode disturbance rejection control with prescribed performance for robotic manipulators. ISA Trans 2019;91:41–51. doi:10.1016/j.isatra.2019.01.017.

[27] Chang L, Jing Y, Liu Y. Design of adaptive h-infinity, controller for power system based on prescribed performance. ISA Trans 2019;100:244–50. doi:10.1016/j.isatra.2019.11.030.

[28] Gai W, Wang H, Zhang J, Li Y. Adaptive neural network dynamic inversion with prescribed performance for aircraft flight control. J Appl Math 2013;2013:452653–. doi:10.1155/2013/452653; publisher: Hindawi Publishing Corporation.

[29] Yang Q, Chen M. Adaptive neural prescribed performance tracking control for near space vehicles with input nonlinearity. Neurocomputing 2016;174:780–9. doi:10.1016/j.neucom.2015.09.099.

[30] Zhu G, Liu J. Neural network-based adaptive backstepping control for hypersonic flight vehicles with prescribed tracking performance. Math Probl Eng 2015;2015:591789–. doi:10.1155/2015/591789; publisher: Hindawi Publishing Corporation.

[31] Wang W, Wen C. Adaptive actuator failure compensation control of uncertain nonlinear systems with guaranteed transient performance. Automatica 2010;46(12):2082–91. doi:10.1016/j.automatica.2010.09.006.

[32] Chen M, Wu Q, Jiang C, Jiang B. Guaranteed transient performance based control with input saturation for near space vehicles. Sci China-Inf Sci 2014;57(5):52204–. doi:10.1007/s11432-013-4883-9.

[33] Bu X, Wu X, Zhu F, Huang J, Ma Z, Zhang R. Novel prescribed performance neural control of a flexible air-breathing hypersonic vehicle with unknown initial errors. ISA Trans 2015;59:149–59. doi:10.1016/j.isatra.2015.09.007.

[34] Wu D, Chen M, Ye H. High angle of attack flight control based on switched prescribed performance. Int J Adapt Control Signal Process 2020;34(8):1059–79. doi:10.1002/acs.3119.

[35] Wang Y, Hu J. Improved prescribed performance control for air-breathing hypersonic vehicles with unknown deadzone input nonlinearity. ISA Trans 2018;79:95–107. doi:10.1016/j.isatra.2018.05.008.

[36] Keshmiri S, Colgren R, Mirmirani M. Six dof nonlinear wquations of motion for a generic hypersonic vehicle. In: AIAA Atmospheric Flight Mechanics Conference and Exhibit. 2007, p. 6626–53.

[37] Keshmiri S, Mirmirani M, Colgren RD. Six-dof modeling and simulation of a generic hypersonic vehicle for conceptual design studies. In: AIAA modeling and simulation technologies conference and exhibit. 2004, p. 4805–16.

[38] Fallaha CJ, Saad M, Kanaan HY, Al-Haddad K. Sliding-mode robot control with exponential reaching law. IEEE Trans Ind Electron 2011;58(2):600–10. doi:10.1109/TIE.2010.2045995; conference Name: IEEE Transactions on Industrial Electronics.

## Appendix A.

$$
\begin{cases}
\bar{G}_\alpha = m_0 g \cos\gamma \cos\mu \\
\bar{G}_\beta = m_0 g \cos\gamma \sin\mu \\
\bar{G}_\mu = -m_0 g \cos\gamma \tan\beta \cos\mu
\end{cases}
\qquad
\begin{cases}
F_{d\alpha} = -F_{dL} \\
F_{d\beta} = F_{dY} \\
F_{d\mu} = F_{dL}(\tan\beta + \tan\gamma \sin\mu) + F_{dY} \tan\gamma \cos\mu
\end{cases}
\tag{A.1}
$$

$$\begin{cases} f_q = \dfrac{(J_z - J_x)\, pr}{J_y} + \dfrac{\bar{q}cS\left(C_{m\alpha} + C_{mq}qc/(2V)\right)}{J_y} + \dfrac{x_{cg}\bar{q}S\left(C_{D\alpha}\sin\alpha + C_{L\alpha}\cos\alpha\right)}{J_y} \\ f_r = \dfrac{(J_x - J_y)\, pq}{J_z} + \dfrac{\bar{q}bSC_{n\beta}\beta - x_{cg}\bar{q}SC_{Y\beta}}{J_z} + \dfrac{\bar{q}bS\left(C_{nr}rb/(2V) + C_{np}pb/(2V)\right)}{J_z} \\ f_p = \dfrac{(J_y - J_z)\, qr}{J_x} + \dfrac{\bar{q}bSC_{l\beta}\beta}{J_x} + \dfrac{\bar{q}bS\left(C_{lp}pb/(2V) + C_{lr}rb/(2V)\right)}{J_x} \end{cases} \tag{A.2}$$

$$\boldsymbol{g}_s = \begin{bmatrix} 1 & -\sin\alpha\tan\beta & -\cos\alpha\tan\beta \\ 0 & -\cos\alpha & \sin\alpha \\ 0 & \sin\alpha\sec\beta & \cos\alpha\sec\beta \end{bmatrix} \tag{A.3}$$

$$\boldsymbol{g}_f = J^{-1}\bar{q}S \begin{bmatrix} g_{q\delta_e} & g_{q\delta_a} & g_{q\delta_r} \\ g_{r\delta_e} & g_{r\delta_a} & g_{r\delta_r} \\ g_{p\delta_e} & g_{p\delta_a} & g_{p\delta_r} \end{bmatrix} \tag{A.4}$$